 doi:10.20944/preprints202206.0236.v1

Article

BAP1 loss promotes suppressive tumor immune microenvironment via up-regulation of PROS1 in class 2 uveal melanomas

Christopher J. Kaler[1], James J. Dollar[1], Anthony M. Cruz[1], Jeffim N. Kuznetsoff[1], Margaret l. Sanchez[1], Christina L. Decatur[1], Jonathan D. Licht[2], Keiran S.M. Smalley[3], Zelia M. Correa[1], Stefan Kurtenbach[1], and J. William Harbour[1,4]*

1 Bascom Palmer Eye Institute, Sylvester Comprehensive Cancer Center and Interdisciplinary Stem Cell Institute, University of Miami Miller School of Medicine, Miami, FL USA
2 University of Florida Health Cancer Center, University of Florida Cancer and Genetics Research Complex, Gainesville, FL, USA.
3 Department of Tumor Biology, Moffitt Cancer Center & Research Institute, Tampa, FL, USA.
4 Department of Ophthalmology and Harold C. Simmons Comprehensive Cancer Center, University of Texas Southwestern Medical Center, Dallas, TX USA

* Correspondence: William.Harbour@UTSouthwestern.edu; Tel.: (214) 648-2304

Simple Summary:

Abstract: Uveal melanoma (UM) is the most common primary cancer of the eye and is associated with a high rate of metastatic death. UM can be stratified into two main classes based on metastatic risk, with class 1 UM having a low metastatic risk and class 2 UM having a high metastatic risk. Class 2 UM have a distinctive genomic, transcriptomic, histopathologic, and clinical phenotype characterized by biallelic inactivation of the *BAP1* tumor suppressor gene, an immune suppressive microenvironment enriched for M2-polarized macrophages, and poor response to checkpoint inhibitor immunotherapy. To identify potential mechanistic links between BAP1 loss and immune suppression in class 2 UM, we performed an integrated analysis of UM samples, as well as genetically engineered UM cell lines and uveal melanocytes (UMC). Using RNA sequencing (RNA-seq), we found that the most highly up-regulated gene associated with BAP1 loss across these datasets was *PROS1*, which encodes a ligand that triggers phosphorylation and activation of the immunosuppressive macrophage receptor MERTK. The inverse association between *BAP1* and *PROS1* in class 2 UM was confirmed by single-cell RNA-seq, which also revealed that *MERTK* was up-regulated in CD163+ macrophages in class 2 UM. Using ChIP-seq, BAP1 knockdown in UM cells resulted in an accumulation of H3K27ac at the *PROS1* locus, suggesting epigenetic regulation of *PROS1* by BAP1. Phosphorylation of MERTK in RAW 264.7 monocyte-macrophage cells was increased upon co-culture with $BAP1^{-/-}$ UMCs, and this phosphorylation was blocked by depletion of PROS1 in the UMCs. These findings were corroborated by multi-color immunohistochemistry, where class 2/BAP1-mutant UMs demonstrated increased PROS1 expression in tumor cells and increased MERTK phosphorylation in CD163+ macrophages compared to class 1/BAP1-wildtype UMs. Taken together, these findings provide a mechanistic link between BAP1 loss and suppression of the tumor immune microenvironment in class 2 UMs, and they implicate the PROS1-MERTK pathway as a potential target for immunotherapy in UM.

Keywords: uveal melanoma, BAP1, PROS1, MERTK, macrophage, tumor immune microenvironment, metastasis

 doi:10.20944/preprints202206.0236.v1

1. Introduction

Uveal melanoma (UM) is the most common primary cancer of the eye and is often associated with fatal metastasis [1]. UM can be stratified into two prognostically significant subtypes, with class 1 UM having a low metastatic risk and class 2 UM a high metastatic risk [2,3]. Biallelic inactivation of the tumor suppressor *BAP1* is the distinctive genomic feature of class 2 UM, which occurs through mutation of one allele and whole chromosome loss of the other allele [4].

Despite increasingly effective management of primary UM, there has been no corresponding improvement in patient survival [5], due to a propensity for early micrometastasis and immune escape [6]. UM is an immunologically "cold" tumor type that responds poorly to checkpoint inhibitor immunotherapy [7], which is due at least in part to a suppressive tumor immune microenvironment (TIME), including an enrichment of M2 polarized (M2) macrophages, T cells expressing checkpoint or "exhaustion" markers, and increased HLA expression on tumor cells [8-12]. Importantly, the suppressive TIME in UM is strongly associated with mutational inactivation of *BAP1* [8,9,13], suggesting a mechanistic link between genomic abberations and immune suppression.

While it is now widely recognized that the TIME plays a critical role in cancer progression and therapeutic resistance [14], how the tumor genome shapes the TIME remains poorly understood. Here, we used an integrative approach to explore the mechanistic relationship between *BAP1* mutations and the TIME in UM.

2. Materials and Methods

2.1. Cell Lines

UMC026 cells with and without CRISPR-Cas9 mediated deletion of the first exon of BAP1 (*BAP1*$^{-/-}$) were established and cultured in our laboratory from normal uveal melanocytes in a patient undergoing enucleation as previously described [15]. RAW 264.7 monocyte-macrophage like cells (ATCC, Manassas, Virginia) were grown in DMEM media with 10% Tet-Free FBS at 37°C in 20% oxygen and 5% CO2. MP41 and MP46 cells were a kind gift from Dr. Sergio Roman-Roman [16] and were cultured as previously described [17]. Mel202 and 92.1 were gifts from Drs. B. Ksander and M. Jager, respectively. UMC026, 92.1, Mel202 and MP41 were engineered to allow tet-inducible knockdown of BAP1 as previously described [18]. The BAP1-mutant cell line MP46 UM was engineered to allow for tet-inducible expression of exogenous BAP1 by stable lentiviral integration of pLV-TET-HA-BAP1-WT and pLVX-TET-ON (Clontech) constructs. pLV-TET-HA-BAP1-WT was created by PCR amplification and subsequent recombination of a full length BAP1 cDNA fragment into pLV-TET-PURO (Addgene #26430). The plasmids were packaged into lentiviral particles by transient co-transfection into HEK293T cells with pMD2G and psPAX2 packaging plasmids using JetPrime reagent (Polyplus), and the virally transduced MP46 cells selected with puromycin (2 ug/mL) and geneticin (500 ug/mL).

2.2. RNA Sequencing (RNA-seq)

RNA-seq was performed as previously described [18]. Briefly, RNA was isolated with Direct-zol RNA kit (Zymo), and melanin pigment was removed using OneStep PCR Inhibitor Removal Kit (Zymo), according to the manufacturers' instructions. Libraries were prepared and sequencing was performed by the Sylvester Comprehensive Cancer Center Oncogenomics Shared Resource at the University of Miami. Sequencing quality was assessed using FastQC (v0.11.3). Reads were trimmed using Trim Galore! [19], aligned to the human genome build hg38/GRCH38 using STAR [20] and counts were generated using RSEM [21]. Venn diagram was generated by overlap of RNA-seq datasets included genes with >30% up-regulation, and FPKM > 10. Significance of PROS1 expression in shBAP1 and BAP1 tumor samples was calculated with a ratio paired t-test of normalized read counts across all datasets.

 doi:10.20944/preprints202206.0236.v1

2.3. Immunoblotting

Immunoblotting was performed as previously described [17,18]. Briefly, cells were harvested from culture dishes, suspended in RIPA buffer with protease and phosphatase inhibitors on ice, sonicated at 50% power for 10 seconds on ice, and protein quantified by BCA assay. Equivalent cell protein quantities were mixed with 1% SDS, heated for 10 minutes at 75˚C and electrophoresed through TGX polyacrylamide gels (Bio-Rad; Hercules, California), or frozen at -20˚C. Primary antibodies included anti-BAP1 (Santa Cruz Biotechnologies, Dallas, Texas, sc-28383), anti-PROS1 (Catalogue #16910-1-AP, Proteintech, Rosemont, Illinois), or anti-β-actin (Catalogue #66009-1-IG, Proteintech, Rosemont, Illinois) antibodies and HRP secondary antibodies (Catalogue #7076S and 7074P2, Cell Signaling Technology, Danvers, Massachusetts). Blot imaging was performed with the Bio-Rad ChemiDoc XRS Imaging System (Bio-Rad, Hercules, California) and densitometric signal quantitation was performed using ImageJ (https://imagej.nih.gov/ij/).

2.4. ChIP-seq

Chromatin immunoprecipitation (ChIP) followed by next-generation sequencing (ChIP-seq) was performed using 20 million cells per experiment, which were crosslinked for 7 minutes with 1% formaldehyde. Chromatin was sonicated to an average fragment size of 200-500 base pairs with a Covaris M220 sonicator. 10 μg of antibody was used for each ChIP experiment. Libraries were prepared using the NEBNext Ultra 2 kit and sequenced by the University of Miami Oncogenomics Shared Resource with > 20 million reads per sample. Reads were quality filtered by Trim Galore! [19] and aligned to the hg38 genome with Bowtie2 [23]. Normalized coverage tracks were generated with MACS2 [24], and plotted with SparK [25].

2.5. Single-cell RNA sequencing (scRNA-seq)

A total of 59,915 cells from 11 UM samples were analyzed by scRNA-seq as previously described [8]. Using the first 20 principal components of variably expressed genes, dimensionality reduction was conducted with Seurat (version 4.1.0) using Uniform Manifold Approximation and Projection (UMAP) methodology [26,27]. Cell type annotations were assigned as previously described [8]. Differentially expressed genes were identified using Wilcoxon Rank Sum test of log normalized counts. Dimensional reduction plots, dot plots, and scatter plots were generated using Seurat. Significance of correlation between expression of genes was conducted in R using Spearman's rank-based measure of association.

2.6. ELISA

Media was collected from cell culture plates following 72 h incubation of UMC026 cells with and without BAP1 knockout. Media samples (1 ml) were centrifuged at 1,000 g for 10 minutes, and 800 μl removed and frozen at -80˚C. Cell count was determined for each culture plate by trypsinization of cells (2 ml, 0.5% trypsin) and quantification by spectrophotometer. PROS1 protein quantification was performed using a commercially validated enzyme-linked immunosorbent assay (Catalogue # MBS9427967, MyBioSource, Inc., San Diego, California,) for three different sets of media from UMC026 cells with and without BAP1 knockout. ELISA measurements were performed in triplicate using a VersaDoc spectrophotometer instrument (Bio-Rad; Hercules, California).

2.7. Confocal Immunocytochemistry

UMC026 cells with and without BAP1 knockout were grown in culture on glass coverslips coated with poly-L-lysine. Cells were fixed in 4% paraformaldehyde (v/v in PBS) for 10 minutes, washed 2x in PBS and incubated in 0.8% glycine (v/v in PBS) for 10 minutes. Cells

Preprints (www.preprints.org) | NOT PEER-REVIEWED | Posted: 16 June 2022 doi:10.20944/preprints202206.0236.v1

were then permeabilized for 30 minutes in 0.05% Tween-20 (v/v in PBS), incubated in 0.27% ammonium chloride (v/v in PBS) for 10 minutes, and washed 3x in PBS. Cells were blocked with 5% BSA, 1% NGS and 0.5% Tween-20 (v/v in TBS) for 1 hour and washed 3x in TBS. Cells were incubated in anti-PROS1 primary antibody (Proteintech, Rosemont, Illinois, 16910-1-AP) overnight at 4°C, washed 3x in TBS and then incubated in secondary antibody (Cell Signaling Technology, Danvers, Massachusetts, 7074P2) for 1 hours at room temperature. Samples were then washed 3x in TBS, mounted with SlowFade Diamond Antifade mounting medium with DAPI (Thermo Fischer Scientific, Waltham, Massachusetts), and imaged using an SP8 Leica laser scanning confocal microscope (Leica Microsystems Inc, Buffalo Grove, IL).

2.8. Multicolor Immunohistochemistry

Multicolor immunohistochemistry was performed using HistoWiz Inc. (Brooklyn, NY). Samples were fixed in formalin, embedded in paraffin, and placed onto glass slides in 4 μm sections. Sequential tyramide (Akoya OPAL) based immunofluorescence was performed on a Bond Rx autostainer (Leica Biosystems, Deer Park, IL) with EDTA pH 9.0 Heat Induced Epitope Retrieval (HIER) for 40 minutes. Antibodies used sequentially included: phospho-MERTK (Cataogue #PMKT-140AP, FabGennix, Frisco, Texas) at 1:50 dilution, PROS1 (Catalogue # ab280885, Abcam, Waltham, Massachusetts) at 1:175 dilution, CD163 (Histowiz, Brooklyn, NY) at 1:100 dilution, and BAP1 (Catalogue # ab255611, Abcam, Waltham, Massachusetts) at 1:100) dilution. Slides were counterstained with DAPI, then coverslipped with Prolong Diamond Antifade Mounting Medium (Catalogue # P36961, Thermo Fischer Scientific, Waltham, Massachusetts) to prevent bleaching and signal loss. Whole slide scanning (20x) was performed on an Akoya Polaris IF Scanner (Akoya Biosciences, Marlborough, Massachusetts) with matching OPAL filters o570, o620, o480 and o520. VisioPharm Artificial Intelligence (AI) image analysis (VisioPharm, Hoersholm, Denmark) was performed on 60 regions of interest measuring 466μm x 349μm from class 1 (UMM065, UMM079) and class 2 (UMM063, UMM069) primary UM samples. A total of 91,532 cells were analyzed and the percentage of cells staining positive for BAP1, PROS1, CD163, and Phospho-MERTK was determined. Additionally, the percentage of cells that co-stained for CD163 and phospho-MERTK was determined.

2.9. Co-Culture Experiments

MERTK activation in RAW 264.7 cells was assessed by immunoprecipitation and immunoblot as previously described [28] following 12 hour co-culture with $BAP1^{+/+}$ or $BAP1^{-/-}$ UMC026 cells, or $BAP1^{-/-}$ UMC026 cells treated with siRNA against PROS1 or with non-targeting control siRNA using commercially validated siRNA oligonucleotides and lipofectamine RNAi max reagents (Thermo Fischer Scientific, Carlsbad CA). Co-culture was initiated 48-72 hours after treatment with siRNA. UMC026 cells (2.5×10^6) were cultured alone or with RAW 264.7 cells (2.5×10^6; plated 24 h prior) in DMEM media with 10% Tet-Free FBS at 37C in 20% oxygen and 5% CO2 for 12 hours. Co-cultures were treated with 120μM pervanadate (prepared fresh by combining 20 mM sodium orthovanadate in 0.9× PBS in a 1:1 ratio with 0.3% hydrogen peroxide in PBS for 15–20 min at room temperature) for 3 min prior to collection. Cell lysates were prepared in 50 mM HEPES (pH 7.5), 150 mM NaCl, 10 mM EDTA, 10% glycerol, and 1% Triton X-100, supplemented with protease inhibitors (Sigma-Aldrich, St. Louis, MO). MERTK was immunoprecipitated with anti-Mer (R&D Systems, Minneapolis, MN) and Protein G beads. Phospho-MERTK was detected by immunoblotting using an anti-phospho-Mer (FabGennix, Frisco, TX) antibody. Nitrocellulose membranes were then stripped, and pan-MERTK detected using anti-Mer antibody (R&D Systems, Minneapolis, MN). The co-culture experiments were performed in triplicate and the ratios of phosphorylated- to pan-MERTK protein levels were obtained by densitometry using ImageJ.

Preprints (www.preprints.org) | NOT PEER-REVIEWED | Posted: 16 June 2022 doi:10.20944/preprints202206.0236.v1

2.10. Statistical Analysis

Two-tailed t-test was used for continuous data and chi square analysis for categorical data, using GraphPad Prism software version 8.0 for Windows, GraphPad Software (San Diego, CA, USA, www.graphpad.com). For scRNA-seq differential expression analysis, two-sided non-parametric Wilcoxon rank sum test with Bonferroni correction using all genes was used. Pearson correlation was used for correlating expression between genes.

Accession Codes

Submission of the RNA-Seq and ChIP-seq data generated in this study to the Gene Expression Omnibus is in process.

3. Results

BAP1 Regulates PROS1 By Epigenetic Mechanisms

To identify genes regulated by BAP1, we analyzed RNA-seq data for differentially expressed genes in three UM cell lines (92.1, Mel202, MP41) and one cell line derived from normal human uveal melanocytes (UMC026) following shRNA knockdown of BAP1, and in 80 human UMs from The Cancer Genome Atlas (TCGA) database that were wildtype versus mutant for BAP1. By plotting genes with 30% increase in FPKM and a minimum of 10 FPKM, we found that only two genes were up-regulated across all of these datasets, *PROS1* and *GDF15* (**Figure 1A**), both of which have been linked to immune suppressive macrophage polarization [29,30]. Up-regulation was significant for both *PROS1* (p=0.0027) and *GDF15* (p=0.0194) when comparing BAP1-competent to BAP1-deficient samples across all datasets. Here, we focused on *PROS1* and its potential role in suppressing the TIME in BAP1-deficient UM. Deletion of BAP1 in UMC026 cells and knockdown of BAP1 in Mel202 cells resulted in up-regulation of PROS1, whereas ectopic expression of BAP1 in BAP1-deficient MP46 cells resulted in down-regulation of PROS1 (**Figure 1B, Supplementary Figure S1**). Further, knockdown of BAP1 resulted in increased acetylation of histone H3 at lysine 27 (H3K27ac) around the *PROS1* locus (**Figure 1C**). These findings suggest that BAP1 represses *PROS1* at least in part by epigenetic mechanisms, and that BAP1 loss leads to increased *PROS1* expression.

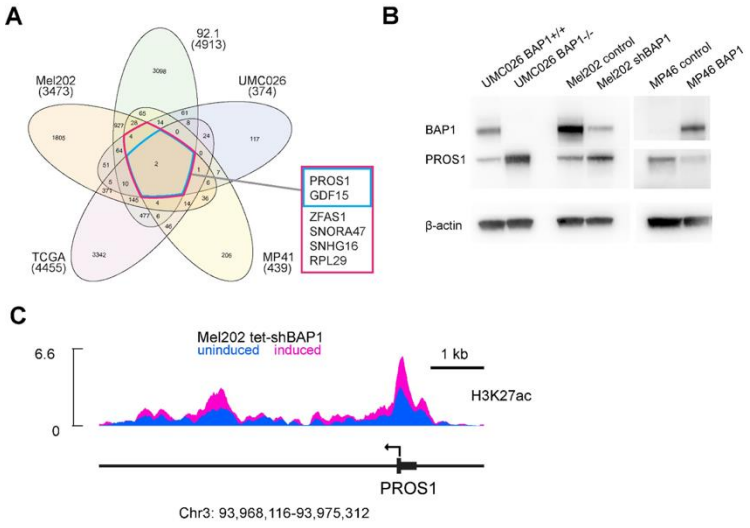

Figure 1. PROS1 expression is regulated by BAP1 in uveal melanocytes and uveal melanoma cells. (**A**) Summary of RNA sequencing data from BAP1-wildtype Mel202, 92.1 and MP41 uveal melanoma cells, and UMC026 uveal melanocytes with or without shRNA-mediated knockdown of BAP1, and 80 UM samples from the Cancer Genome Atlas (TCGA) data repository with or without mutational inactivation of BAP1. Numbers in parenthesis

Preprints (www.preprints.org) | NOT PEER-REVIEWED | Posted: 16 June 2022 doi:10.20944/preprints202206.0236.v1

indicate the number of genes up-regulated by loss of BAP1. Numbers within the Venn diagram indicate the number of overlapping genes between indicated subsets of genes. PROS1 was one of only two genes that was up-regulated across all datasets. (**B**) Immunoblots confirming up-regulation of PROS1 protein following knock-out of BAP1 in UMC026 cells, or knockdown of BAP1 in Mel202 cells. Conversely, ectopic expression of BAP1 in MP46 BAP1-mutant class 2 uveal melanoma cells resulted in down-regulation of PROS1. (**C**) ChIP-seq analysis of H3K27ac at the PROS1 locus in Mel202 cells with or without doxycycline-induced shRNA-mediated knock-down of BAP1.

Single-Cell Sequencing Analysis of PROS1 and MERTK in Uveal Melanomas

To further explore the relationship between BAP1 and PROS1, we analyzed single-cell RNA sequencing from 11 human UM samples, as previously described [8](**Figure 2A**). There was a strong association between BAP1-mutant class 2 tumors and PROS1 expression (adj. P-value < 10^{-300}) (**Figure 2B**). We then performed a further analysis limited to tumor associated macrophages, which clustered according to GEP class (**Figure 2C**). Macrophages derived from class 2 tumors demonstrated significantly increased expression of the macrophage receptor tyrosine kinase *MERTK* (adj. P-value = $1.5x10^{-9}$) (**Figure 2D**), which was strongly associated with expression of the M2 polarization marker CD163 (adj. P-value $1.1x10^{-12}$) (**Figure 2E)**.

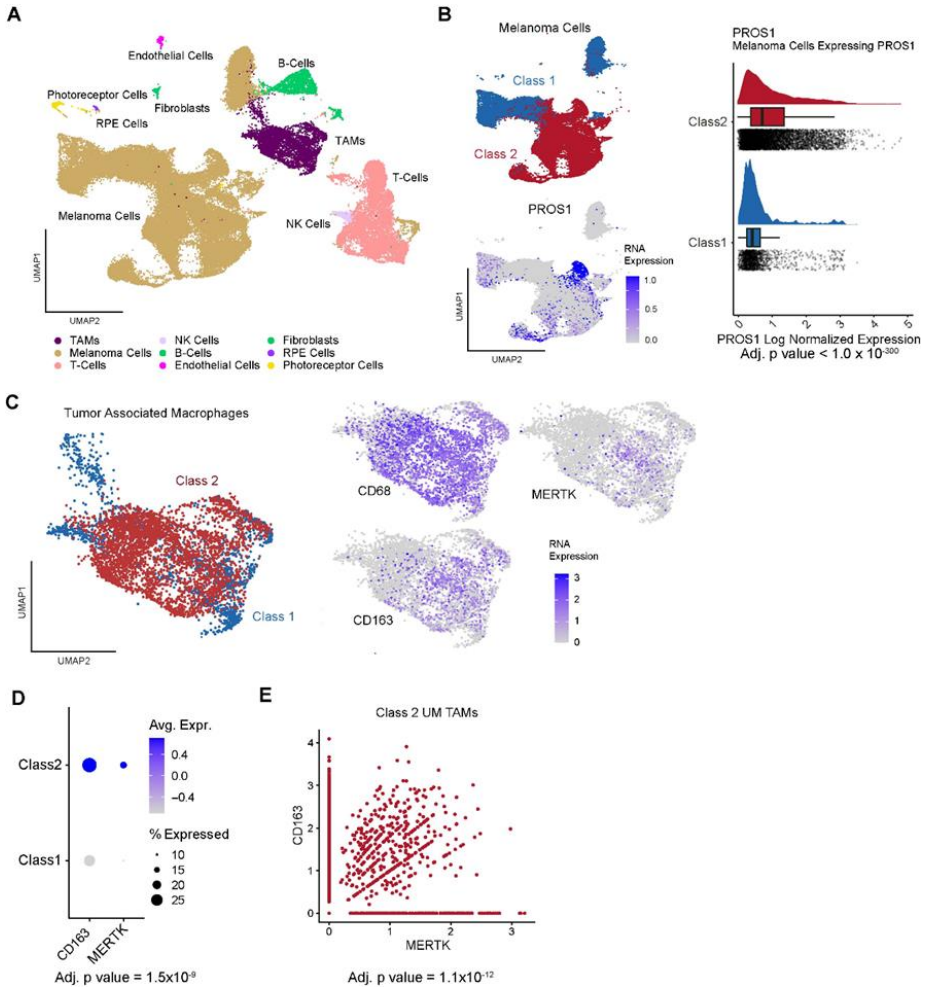

Figure 2. Single-cell RNA sequencing analysis of *PROS1* and *MERTK* in uveal melanomas. (**A**) UMAP dimensionality reduction plot of 59,915 neoplastic and non-neoplastic cells from 11 uveal melanoma samples, with cell types indicated in the legend. (**B**) Left, UMAP plot of the 42,230 uveal melanoma cells in the dataset, with colors indicating gene expression profile (GEP) class 1 (*blue*) and class 2 (*red*). Right, corresponding UMAP plot demonstrating log normalized expression of *PROS1*, as indicated by heatmap. (**C**) Left, UMAP plot of the 5,053 monocytes/macrophages in the dataset, with colors indicating GEP class 1 (*blue*) and class 2 (*red*) of the tumors from which the cells were derived. Right, corresponding UMAP plots demonstrating log normalized expression

 doi:10.20944/preprints202206.0236.v1

of *CD68*, *CD163* and *MERTK*, as indicated by heatmap. (**D**) Dot plot demonstrating *MERTK* expression in monocytes/macrophages with respect to GEP class status of the tumors from which the cells were derived. (**E**) Scatter plot demonstrating association between expression of MERTK and CD163 in monocytes/macrophages from class 2 tumors.

PROS1 Up-Regulation Following BAP1 Loss Triggers MERTK Phosphorylation in Macrophages

PROS1 can function as a secreted protein, and it can also be localized to the cell membrane and cytoplasm [31-34]. In UMC026 cells, knockout of BAP1 did not result in an increase in secreted PROS1 in the cell culture media (**Figure 3A, Supplementary Figure S2**), whereas we found PROS1 localized to the cell membrane and cytoplasm (**Figure 3B**), suggesting that it may function through cell-cell interaction rather than paracrine signaling in this setting. PROS1 is known to promote M2 macrophage polarization by stimulating phosphorylation of the MERTK receptor [29,34-36]. Thus, we performed co-culture experiments to study the effect of BAP1 loss in UMC026 cells on MERTK phosphorylation in RAW 264.7 monocyte-macrophage cells [37,38]. Indeed, BAP1 knockout in UMC026 cells resulted in a significant increase in MERTK phosphorylation in RAW 264.7 cells (**Figure 3C-D**), which was blocked by knockdown of PROS1 in BAP1-KO UM026 cells (**Figure 3E-F** and **Supplementary Figure S3**).

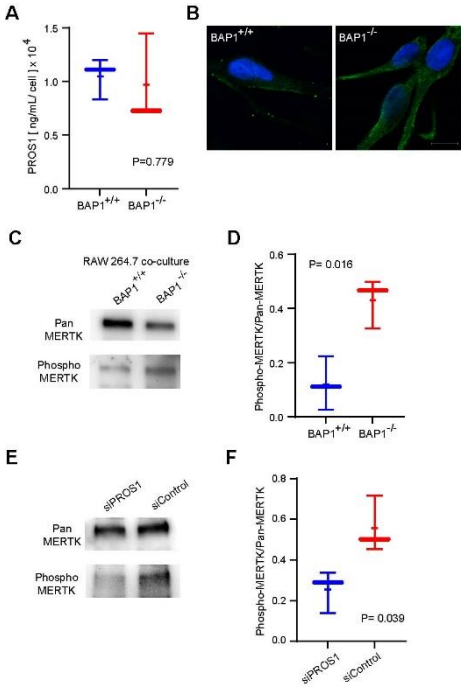

Figure 3. Loss of BAP1 in uveal melanocytes activates MERTK in macrophages in a manner dependent on PROS1. (**A**) Soluble PROS1 protein levels measured by ELISA in media from cultured UMC026 cells with or without knockout of BAP1. (**B**) Confocal microscopy of UMC026 cells with or without knockout of BAP1 immunostained for PROS1. (**C**) Representative immunoblot of lysates from RAW 264.7 cells co-cultured with UMC026 cells with or without knockout of BAP1, immunoprecipitated with pan-MERTK antibody and probed with phospho-MERTK antibody. Immunoprecipitated MERTK is undetectable when UMC026 cells are cultured independently of RAW 264.7 cells (**Supplementary Figure S4**) (**D**) Densitometric analysis of immunoblots from triplicate co-culture experiments represented in panel C. (**E**) Representative immunoblot of lysates from RAW 264.7 cells co-cultured with UMC026 cells knocked out for BAP1, with or without siRNA-mediated knockdown of PROS1, immunoprecipitated with pan-MERTK antibody and probed with phospho-MERTK antibody. (**F**) Densitometric analysis of immunoblots from triplicate co-culture experiments represented in panel E.

Preprints (www.preprints.org) | NOT PEER-REVIEWED | Posted: 16 June 2022 doi:10.20944/preprints202206.0236.v1

Consistent with these findings, multicolor immunohistochemistry in human class1/BAP1-wildtype and class2/BAP1-mutant UM samples revealed a significant association between BAP1 loss and PROS1 up-regulation in UM cells and MERTK phosphorylation in tumor-associated macrophages (**Table 1**, **Figure 4A** and **Supplementary Figure S5-S8**). Further, macrophages expressing the M2 polarization marker CD163 were enriched in BAP1-mutant UM samples as previously reported [39]. In BAP1-mutant UM samples, the subset of CD163-positive cells also positive for phospho-MERTK (double-positive cells) was significantly higher than in class 1 UM cells (**Figure 4B**), consistent with increased MERTK signaling in immune suppressive macrophages of BAP1-mutant vs BAP1-wildtype UM.

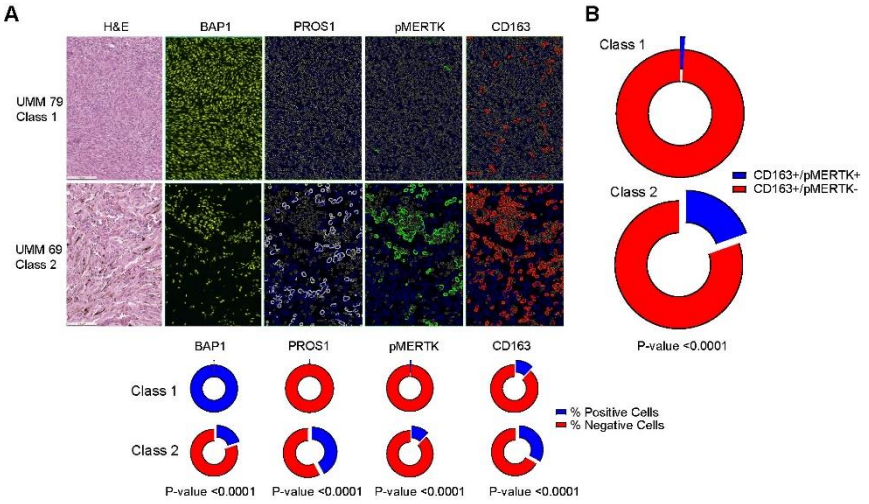

Figure 4. Multi-color immunohistochemistry of PROS1, MERTK and CD163 in uveal melanomas. (A) Top, representative photomicrographs of class 1 and class 2 uveal melanomas analyzed with hematoxylin and eosin (H&E) and with immunostaining for BAP1, PROS1, phosphorylated MERTK (phospho-MERTK), and CD163. Bottom, donut plots summarizing percentage of cells that were positive for each biomarker with respect to GEP tumor class 1 versus class 2. (**B**) Donut plot demonstrating the proportion of CD163+/phospho-MERTK+ cells with respect to GEP tumor class 1 versus class 2.

Table 1. Summary of multi-color immunohistochemistry in primary uveal melanomas

	Number of cells[a]	BAP1[b]	PROS1	Phospho-MerTK	CD163	CD163 and Phospho-MerTK
Class 1	59,990	59,945 (99.93%)	43 (0.072%)	496 (0.83%)	7,098 (11.89%)	77 (1.09%)
Class 2	31,542	6,289 (19.94%)	13,301 (42.17%)	3,889 (12.27%)	10,476 (33.06%)	2,051 (19.58%)
P-value	NA	<0.0001	<0.0001	<0.0001	<0.0001	<0.0001

[a] Total number of cells analyzed from two class 1 and two class 2 primary uveal melanomas.
[b] Number (and percentage) of cells staining positive for each indicated protein

4. Discussion

Inactivation of BAP1 is the single most consistent mutation associated with metastatic death in UM [4,40], and yet it remains unclear how BAP1 loss promotes metastasis. BAP1

Preprints (www.preprints.org) | NOT PEER-REVIEWED | Posted: 16 June 2022 doi:10.20944/preprints202206.0236.v1

is a deubiquitinating enzyme with many binding partners and substrates, and it has been proposed to affect a wide range of processes such as transcriptional regulation, DNA repair and metabolism [41]. Interestingly, loss of BAP1 in uveal melanocytes and UM cells results only in a subtle phenotype *in vitro* [42], suggesting that the dramatic metastatic phenotype associated with BAP1 loss *in vivo* may be the result of complex multi-cellular interactions that are not adequately captured by cell culture experiments. BAP1-mutant UMs display a suppressive TIME enriched for M2 polarized macrophages and T cells expressing checkpoint or "exhaustion" markers such as LAG3, TIM3 and TIGIT [8,9,13,43], similar to findings in other cancer types [44]. Consequently, BAP1 loss may promote metastasis at least in part by allowing tumor cells to evade the patient's immune response. However, it remains unknown mechanistically how BAP1 mutations may lead to immune suppression.

As a potential explanation, we found here that BAP1 loss results in up-regulation of PROS1 in UM cells through epigenetic mechanisms involving H3K27ac accumulation at the *PROS1* locus, consistent with our previous findings [15]. Up-regulation of PROS1 has also been associated with increased metastatic risk in other cancer types [45-47]. PROS1 is a ligand and agonist of the MERTK receptor [48], which when activated by phosphorylation triggers signaling pathways in macrophages that suppress pro-inflammatory M1 polarization and promote anti-inflammatory M2 polarization [34,36,49]. M2 polarized macrophages lead to further suppression of the TIME by secreting cytokines that inhibit T cells and other immune cell types [35]. Indeed, M2 macrophages may be a primary driver of the suppressive TIME in UM [10], and they are associated with suppression of T cells related to therapeutic resistance to tebentafusp, a T cell redirection therapy and the only FDA approved medication for metastatic UM [50].

The critical role of cancer genomic aberrations in promoting immune evasion, cancer evolution and metastasis has become increasingly apparent [51,52]. Our findings reveal a potential mechanistic link between BAP1 mutations and immune evasion in UM via transcriptionally-mediated increased PROS1 expression and phospho-activation of tumor associated macrophage MERTK receptors (**Figure 5**), and they propose new possibilities for overcoming resistance to immunotherapy in UM. A strength of our study was the use of UMC026 cells derived from normal human uveal melanocytes to validate that our findings were specific to BAP1 loss and not the result of private genomic aberrations peculiar to a specific UM cell line. Indeed, the MERTK inhibitor sitravatinib has been shown to circumvent resistance to immune checkpoint blockade in immunologically "cold" cancer types through its effects on the suppressive TIME [35]. These findings warrant further investigation to explore the potential role for targeting the PROS1-MERTK pathway in UM.

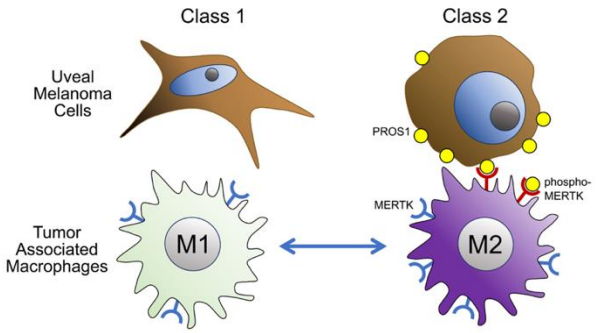

Figure 5. Proposed model for how BAP1 loss leads to suppression of the tumor immune microenvironment. In class 1 BAP1-wildtype uveal melanomas, tumor cells express low levels of PROS1, and tumor associated macrophages are mostly M1 polarized with low MERTK expression and low MERTK phosphorylation. In BAP1-mutant class 2 uveal melanomas, PROS1 is up-regulated since it is no longer repressed by BAP1. Mostly membrane bound PROS1 on tumor cells interacts with MERTK on nearby macrophages, leading to phosphorylation of MERTK and activation of downstream signaling that promotes M2 polarization.

 doi:10.20944/preprints202206.0236.v1

5. Conclusions

Mutational inactivation of BAP1 in UM may lead to a suppressive TIME at least in part by up-regulation of PROS1 in tumor cells and phospho-activation of MERTK in tumor associated macrophages. These findings nominate MERTK as a potential target for inhibition to increase the efficacy of immunotherapy in UM.

Supplementary Materials: Figure S1: Densitometric quantitation of multiple blots for UMC026 and Mel202 cells with and without BAP1 knockout/knockdown, Figure S2: ELISA standard curve documenting linearity of analyte concentration, Figure S3: Confirmation of PROS1 knockdown in UMC026 BAP1-negative cells used in RAW 264.7 cell co-culture functional assays, Figure S4: Immunoprecipitated MERTK expression is undetected when UMC026 cells were cultured without RAW 264.7 cells, Figure S5-S8: Multicolor immunohistochemistry for 60 regions from class 1 (UMM065, UMM079) and class 2 (UMM063, UMM069) uveal melanomas.

Author Contributions: Conceptualization, S.K., J.W.H.; methodology, C.J.K., J.J.D., J.N.K, S.K., J.W.H.; software, J.J.D., S.K.; validation, C.J.K., J.J.D., A.M.C., M.I.S., S.K.; formal analysis, C.J.K., J.J.D., Z.M.C., S.K., J.W.H.; investigation, C.J.K., J.J.D., A.M.C., M.I.S., S.K.; resources, J.W.H.; data curation, C.J.K., J.J.D., S.K.; writing—original draft preparation, C.J.K., J.W.H.; writing—review and editing, C.J.K., J.J.D., J.N.K., C.L.D., J.D.L., K.S.M.S., Z.M.C., S.K., J.W.H.; supervision, Z.M.C., S.K., J.W.H.; project administration C.L.D., Z.M.C., J.W.H.; funding acquisition, C.J.K., J.W.H. All authors have read and agreed to the published version of the manuscript.

Funding: This work was supported by National Cancer Institute grant R01 CA125970 (J.W.H.), R01 CA125970 Diversity Supplement (A.M.C.), Bankhead-Coley Research Program of the State of Florida 7BC05 (J.D.L., K.S.M.S., J.W.H.), Alcon Research Institute Senior Investigator Award (J.W.H.), Research to Prevent Blindness, Inc. Senior Scientific Investigator Award (J.W.H.), Cancer Prevention and Research Institute of Texas Recruitment of Established Investigator Award RR220010 (J.W.H.), Melanoma Research Foundation Established Investigator Award (J.W.H.), Melanoma Research Alliance Team Science Award (J.W.H.), R01 CA256193 (J.D.L., K.S.M.S., J.W.H.), Research to Prevent Blindness Medical Student Eye Research Fellowship (C.J.K.), University of Miami Miller School of Medicine Dean's Research Excellence Award in Medicine (C.J.K.), and a generous gift from Dr. Mark J. Daily (J.W.H.). Bascom Palmer Eye Institute received funding from N.I.H. Grant P30 EY014801 and a Research to Prevent Blindness Unrestricted Grant. Sylvester Comprehensive Cancer Center received funding from N.C.I. Grant P30 CA240139. Simmons Comprehensive Cancer Center received funding from N.C.I. Grant P30 CA240139.

Institutional Review Board Statement: The study was conducted according to the guidelines of the Declaration of Helsinki, and approved by the Institutional Review Board of the University of Miami (protocol 20120773, original approval date 01/5/2013).

Informed Consent Statement: Informed consent was obtained from all subjects involved in the study.

Data Availability Statement: Submission of the RNA-Seq and ChIP-seq data generated in this study to the Gene Expression Omnibus is in process.

Acknowledgments: We are grateful to the patients who generously contributed samples for this research. We gratefully acknowledge Deborah DeRyckere and Douglas Graham, Emory University, for helpful advice on phospho-MERTK activation assays.

Conflicts of Interest: J.W.H. is the inventor of intellectual property related to prognostic testing in uveal melanoma. He is a paid consultant for Castle Biosciences, licensee of this intellectual property, and he receives royalties from its commercialization. All remaining authors declare no competing financial interests. Castle Biosciences had no role in the design of the study; in the collection, analyses, or interpretation of data; in the writing of the manuscript, or in the decision to publish the results.

References

1. Harbour, J.W.; Shih, H.A. Initial management of uveal and conjunctival melanomas. In *UpToDate, Waltham, MA. (Accessed on April 19, 2022).* Atkins, M.B., Berman, R.S., Eds.; 2018.

2. Onken, M.D.; Worley, L.A.; Char, D.H.; Augsburger, J.J.; Correa, Z.M.; Nudleman, E.; Aaberg, T.M., Jr.; Altaweel, M.M.; Bardenstein, D.S.; Finger, P.T.; et al. Collaborative Ocular Oncology Group report number 1: prospective validation of a multi-gene prognostic assay in uveal melanoma. *Ophthalmology* **2012**, *119*, 1596-1603, doi:10.1016/j.ophtha.2012.02.017.
3. Harbour, J.W.; Chen, R. The DecisionDx-UM Gene Expression Profile Test Provides Risk Stratification and Individualized Patient Care in Uveal Melanoma. *PLoS Curr* **2013**, *5*, doi:10.1371/currents.eogt.af8ba80fc776c8f1ce8f5dc485d4a618.
4. Harbour, J.W.; Onken, M.D.; Roberson, E.D.; Duan, S.; Cao, L.; Worley, L.A.; Council, M.L.; Matatall, K.A.; Helms, C.; Bowcock, A.M. Frequent mutation of BAP1 in metastasizing uveal melanomas. *Science* **2010**, *330*, 1410-1413, doi:10.1126/science.1194472.
5. Aronow, M.E.; Topham, A.K.; Singh, A.D. Uveal Melanoma: 5-Year Update on Incidence, Treatment, and Survival (SEER 1973-2013). *Ocular oncology and pathology* **2018**, *4*, 145-151, doi:10.1159/000480640.
6. Eskelin, S.; Pyrhonen, S.; Summanen, P.; Hahka-Kemppinen, M.; Kivela, T. Tumor doubling times in metastatic malignant melanoma of the uvea - Tumor progression before and after treatment. *Ophthalmology* **2000**, *107*, 1443-1449, doi:Doi 10.1016/S0161-6420(00)00182-2.
7. Heppt, M.V.; Amaral, T.; Kahler, K.C.; Heinzerling, L.; Hassel, J.C.; Meissner, M.; Kreuzberg, N.; Loquai, C.; Reinhardt, L.; Utikal, J.; et al. Combined immune checkpoint blockade for metastatic uveal melanoma: a retrospective, multi-center study. *J Immunother Cancer* **2019**, *7*, 299, doi:10.1186/s40425-019-0800-0.
8. Durante, M.A.; Rodriguez, D.A.; Kurtenbach, S.; Kuznetsov, J.N.; Sanchez, M.I.; Decatur, C.L.; Snyder, H.; Feun, L.G.; Livingstone, A.S.; Harbour, J.W. Single-cell analysis reveals new evolutionary complexity in uveal melanoma. *Nat Commun* **2020**, *11*, 496, doi:10.1038/s41467-019-14256-1.
9. Figueiredo, C.R.; Kalirai, H.; Sacco, J.J.; Azevedo, R.A.; Duckworth, A.; Slupsky, J.R.; Coulson, J.M.; Coupland, S.E. Loss of BAP1 expression is associated with an immunosuppressive microenvironment in uveal melanoma, with implications for immunotherapy development. *J Pathol* **2020**, doi:10.1002/path.5384.
10. de Lange, M.; Nell, R.J.; Lalai, R.N.; Versluis, M.; Jordanova, E.S.; Luyten, G.P.; Jager, M.J.; van der Burg, S.H.; Zoutman, W.H.; van Hall, T.; et al. Digital PCR-based T Cell Quantification Assisted Deconvolution of the Microenvironment Reveals that Activated Macrophages Drive Tumor Inflammation in Uveal Melanoma. *Mol Cancer Res* **2018**, doi:10.1158/1541-7786.MCR-18-0114.
11. van Essen, T.H.; van Pelt, S.I.; Bronkhorst, I.H.; Versluis, M.; Nemati, F.; Laurent, C.; Luyten, G.P.; van Hall, T.; van den Elsen, P.J.; van der Velden, P.A.; et al. Upregulation of HLA Expression in Primary Uveal Melanoma by Infiltrating Leukocytes. *PLoS One* **2016**, *11*, e0164292, doi:10.1371/journal.pone.0164292.
12. Bronkhorst, I.H.; Jager, M.J. Uveal melanoma: The inflammatory microenvironment. *J Innate Immun* **2012**, doi:10.1159/000334576.
13. Gezgin, G.; Dogrusoz, M.; van Essen, T.H.; Kroes, W.G.M.; Luyten, G.P.M.; van der Velden, P.A.; Walter, V.; Verdijk, R.M.; van Hall, T.; van der Burg, S.H.; et al. Genetic evolution of uveal melanoma guides the development of an inflammatory microenvironment. *Cancer Immunol Immunother* **2017**, *66*, 903-912, doi:10.1007/s00262-017-1991-1.
14. Labani-Motlagh, A.; Ashja-Mahdavi, M.; Loskog, A. The Tumor Microenvironment: A Milieu Hindering and Obstructing Antitumor Immune Responses. *Front Immunol* **2020**, *11*, 940, doi:10.3389/fimmu.2020.00940.
15. Kuznetsov, J.N.; Aguero, T.H.; Owens, D.A.; Kurtenbach, S.; Field, M.G.; Durante, M.A.; Rodriguez, D.A.; King, M.L.; Harbour, J.W. BAP1 regulates epigenetic switch from pluripotency to differentiation in developmental lineages giving rise to BAP1-mutant cancers. *Sci Adv* **2019**, *5*, eaax1738, doi:10.1126/sciadv.aax1738.
16. Amirouchene-Angelozzi, N.; Nemati, F.; Gentien, D.; Nicolas, A.; Dumont, A.; Carita, G.; Camonis, J.; Desjardins, L.; Cassoux, N.; Piperno-Neumann, S.; et al. Establishment of novel cell lines recapitulating the genetic landscape of uveal melanoma and preclinical validation of mTOR as a therapeutic target. *Mol Oncol* **2014**, *8*, 1508-1520, doi:10.1016/j.molonc.2014.06.004.

17. Kuznetsoff, J.N.; Owens, D.A.; Lopez, A.; Rodriguez, D.A.; Chee, N.T.; Kurtenbach, S.; Bilbao, D.; Roberts, E.R.; Volmar, C.H.; Wahlestedt, C.; et al. Dual Screen for Efficacy and Toxicity Identifies HDAC Inhibitor with Distinctive Activity Spectrum for BAP1-Mutant Uveal Melanoma. *Mol Cancer Res* **2021**, *19*, 215-222, doi:10.1158/1541-7786.MCR-20-0434.
18. Field, M.G.; Kuznetsov, J.N.; Bussies, P.L.; Cai, L.Z.; Alawa, K.A.; Decatur, C.L.; Kurtenbach, S.; Harbour, J.W. BAP1 Loss Is Associated with DNA Methylomic Repatterning in Highly Aggressive Class 2 Uveal Melanomas. *Clin Cancer Res* **2019**, doi:10.1158/1078-0432.CCR-19-0366.
19. Felix, K. Babraham Bioinformatics - Trim Galore! **2020**.
20. Dobin, A.; Davis, C.A.; Schlesinger, F.; Drenkow, J.; Zaleski, C.; Jha, S.; Batut, P.; Chaisson, M.; Gingeras, T.R. STAR: ultrafast universal RNA-seq aligner. *Bioinformatics (Oxford, England)* **2013**, *29*, 15-21, doi:10.1093/bioinformatics/bts635.
21. Li, B.; Dewey, C.N. RSEM: accurate transcript quantification from RNA-Seq data with or without a reference genome. *BMC bioinformatics* **2011**, *12*, 323, doi:10.1186/1471-2105-12-323.
22. Love, M.I.; Huber, W.; Anders, S. Moderated estimation of fold change and dispersion for RNA-seq data with DESeq2. *Genome Biol* **2014**, *15*, 550, doi:10.1186/s13059-014-0550-8.
23. Langmead, B.; Salzberg, S.L. Fast gapped-read alignment with Bowtie 2. *Nature methods* **2012**, *9*, 357-359, doi:10.1038/nmeth.1923.
24. Mistry, M.R.K. Peak calling with MACS2. *Introduction to ChIP-Seq using high-performance computing* **2017**.
25. Kurtenbach, S.; Harbour, J.W. SparK: A Publication-quality NGS Visualization Tool. *bioRxiv* **2019**, doi:10.1101/845529.
26. Butler, A.; Hoffman, P.; Smibert, P.; Papalexi, E.; Satija, R. Integrating single-cell transcriptomic data across different conditions, technologies, and species. *Nature biotechnology* **2018**, *36*, 411-420, doi:10.1038/nbt.4096.
27. Stuart, T.; Butler, A.; Hoffman, P.; Hafemeister, C.; Papalexi, E.; Mauck, W.M.; Stoeckius, M.; Smibert, P.; Satija, R. Comprehensive integration of single cell data. *bioRxiv* **2018**, 460147, doi:10.1101/460147.
28. Zhang, W.; DeRyckere, D.; Hunter, D.; Liu, J.; Stashko, M.A.; Minson, K.A.; Cummings, C.T.; Lee, M.; Glaros, T.G.; Newton, D.L.; et al. UNC2025, a potent and orally bioavailable MER/FLT3 dual inhibitor. *J Med Chem* **2014**, *57*, 7031-7041, doi:10.1021/jm500749d.
29. Ubil, E.; Caskey, L.; Holtzhausen, A.; Hunter, D.; Story, C.; Earp, H.S. Tumor-secreted Pros1 inhibits macrophage M1 polarization to reduce antitumor immune response. *J Clin Invest* **2018**, *128*, 2356-2369, doi:10.1172/JCI97354.
30. Bootcov, M.R.; Bauskin, A.R.; Valenzuela, S.M.; Moore, A.G.; Bansal, M.; He, X.Y.; Zhang, H.P.; Donnellan, M.; Mahler, S.; Pryor, K.; et al. MIC-1, a novel macrophage inhibitory cytokine, is a divergent member of the TGF-beta superfamily. *Proc Natl Acad Sci U S A* **1997**, *94*, 11514-11519, doi:10.1073/pnas.94.21.11514.
31. Carrera Silva, E.A.; Chan, P.Y.; Joannas, L.; Errasti, A.E.; Gagliani, N.; Bosurgi, L.; Jabbour, M.; Perry, A.; Smith-Chakmakova, F.; Mucida, D.; et al. T cell-derived protein S engages TAM receptor signaling in dendritic cells to control the magnitude of the immune response. *Immunity* **2013**, *39*, 160-170, doi:10.1016/j.immuni.2013.06.010.
32. Lew, E.D.; Oh, J.; Burrola, P.G.; Lax, I.; Zagorska, A.; Traves, P.G.; Schlessinger, J.; Lemke, G. Differential TAM receptor-ligand-phospholipid interactions delimit differential TAM bioactivities. *Elife* **2014**, *3*, doi:10.7554/eLife.03385.
33. Rothlin, C.V.; Carrera-Silva, E.A.; Bosurgi, L.; Ghosh, S. TAM receptor signaling in immune homeostasis. *Annu Rev Immunol* **2015**, *33*, 355-391, doi:10.1146/annurev-immunol-032414-112103.
34. Myers, K.V.; Amend, S.R.; Pienta, K.J. Targeting Tyro3, Axl and MerTK (TAM receptors): implications for macrophages in the tumor microenvironment. *Mol Cancer* **2019**, *18*, 94, doi:10.1186/s12943-019-1022-2.
35. Du, W.; Huang, H.; Sorrelle, N.; Brekken, R.A. Sitravatinib potentiates immune checkpoint blockade in refractory cancer models. *JCI Insight* **2018**, *3*, doi:10.1172/jci.insight.124184.
36. Wu, H.; Zheng, J.; Xu, S.; Fang, Y.; Wu, Y.; Zeng, J.; Shao, A.; Shi, L.; Lu, J.; Mei, S.; et al. Mer regulates microglial/macrophage M1/M2 polarization and alleviates neuroinflammation following traumatic brain injury. *J Neuroinflammation* **2021**, *18*, 2, doi:10.1186/s12974-020-02041-7.

37. Zhang, B.; Fang, L.; Wu, H.M.; Ding, P.S.; Xu, K.; Liu, R.Y. Mer receptor tyrosine kinase negatively regulates lipoteichoic acid-induced inflammatory response via PI3K/Akt and SOCS3. *Mol Immunol* **2016**, *76*, 98-107, doi:10.1016/j.molimm.2016.06.016.
38. Lee, Y.J.; Han, J.Y.; Byun, J.; Park, H.J.; Park, E.M.; Chong, Y.H.; Cho, M.S.; Kang, J.L. Inhibiting Mer receptor tyrosine kinase suppresses STAT1, SOCS1/3, and NF-κB activation and enhances inflammatory responses in lipopolysaccharide-induced acute lung injury. *J Leukoc Biol* **2012**, *91*, 921-932, doi:10.1189/jlb.0611289.
39. Bronkhorst, I.H.; Ly, L.V.; Jordanova, E.S.; Vrolijk, J.; Versluis, M.; Luyten, G.P.; Jager, M.J. Detection of M2-macrophages in uveal melanoma and relation with survival. *Investigative ophthalmology & visual science* **2011**, *52*, 643-650, doi:10.1167/iovs.10-5979.
40. Robertson, A.G.; Shih, J.; Yau, C.; Gibb, E.A.; Oba, J.; Mungall, K.L.; Hess, J.M.; Uzunangelov, V.; Walter, V.; Danilova, L.; et al. Integrative analysis identifies four molecular and clinical subsets in uveal melanoma. *Cancer Cell* **2017**, *32*, 204-220 e215, doi:10.1016/j.ccell.2017.07.003.
41. Carbone, M.; Harbour, J.W.; Brugarolas, J.; Bononi, A.; Pagano, I.; Dey, A.; Krausz, T.; Pass, H.I.; Yang, H.; Gaudino, G. Biological Mechanisms and Clinical Significance of BAP1 Mutations in Human Cancer. *Cancer Discov* **2020**, *10*, 1103-1120, doi:10.1158/2159-8290.CD-19-1220.
42. Matatall, K.A.; Agapova, O.A.; Onken, M.D.; Worley, L.A.; Bowcock, A.M.; Harbour, J.W. BAP1 deficiency causes loss of melanocytic cell identity in uveal melanoma. *BMC Cancer* **2013**, *13*, 371, doi:10.1186/1471-2407-13-371.
43. Krishna, Y.; Acha-Sagredo, A.; Sabat-Pospiech, D.; Kipling, N.; Clarke, K.; Figueiredo, C.R.; Kalirai, H.; Coupland, S.E. Transcriptome Profiling Reveals New Insights into the Immune Microenvironment and Upregulation of Novel Biomarkers in Metastatic Uveal Melanoma. *Cancers (Basel)* **2020**, *12*, doi:10.3390/cancers12102832.
44. Wang, T.; Lu, R.; Kapur, P.; Jaiswal, B.S.; Hannan, R.; Zhang, Z.; Pedrosa, I.; Luke, J.J.; Zhang, H.; Goldstein, L.D.; et al. An Empirical Approach Leveraging Tumorgrafts to Dissect the Tumor Microenvironment in Renal Cell Carcinoma Identifies Missing Link to Prognostic Inflammatory Factors. *Cancer Discov* **2018**, doi:10.1158/2159-8290.CD-17-1246.
45. Abboud-Jarrous, G.; Priya, S.; Maimon, A.; Fischman, S.; Cohen-Elisha, M.; Czerninski, R.; Burstyn-Cohen, T. Protein S drives oral squamous cell carcinoma tumorigenicity through regulation of AXL. *Oncotarget* **2017**, *8*, 13986-14002, doi:10.18632/oncotarget.14753.
46. Liu, X.; Liu, Y.; Zhao, J.; Liu, Y. Screening of potential biomarkers in uterine leiomyomas disease via gene expression profiling analysis. *Mol Med Rep* **2018**, *17*, 6985-6996, doi:10.3892/mmr.2018.8756.
47. Ning, P.; Zhong, J.G.; Jiang, F.; Zhang, Y.; Zhao, J.; Tian, F.; Li, W. Role of protein S in castration-resistant prostate cancer-like cells. *Endocr Relat Cancer* **2016**, *23*, 595-607, doi:10.1530/erc-16-0126.
48. Tsou, W.I.; Nguyen, K.Q.; Calarese, D.A.; Garforth, S.J.; Antes, A.L.; Smirnov, S.V.; Almo, S.C.; Birge, R.B.; Kotenko, S.V. Receptor tyrosine kinases, TYRO3, AXL, and MER, demonstrate distinct patterns and complex regulation of ligand-induced activation. *J Biol Chem* **2014**, *289*, 25750-25763, doi:10.1074/jbc.M114.569020.
49. Burstyn-Cohen, T.; Maimon, A. TAM receptors, Phosphatidylserine, inflammation, and Cancer. *Cell Commun Signal* **2019**, *17*, 156, doi:10.1186/s12964-019-0461-0.
50. Khanolkar, R.; Naidoo, R.; Güç, E.; Leach, E.; Stanhope, S.; Gascoyne, D.; Collins, L.; Ranade, K.; Benlahrech, A. IL-2 combination with ImmTAC overcomes CD163+ TAM-like M2 macrophage inhibition of ImmTAC-mediated T cell killing of tumor cells. In Proceedings of the Journal for ImmunoTherapy of Cancer, 2021; pp. A600-A600.
51. Massague, J.; Ganesh, K. Metastasis-Initiating Cells and Ecosystems. *Cancer Discov* **2021**, *11*, 971-994, doi:10.1158/2159-8290.CD-21-0010.
52. Davoli, T.; Uno, H.; Wooten, E.C.; Elledge, S.J. Tumor aneuploidy correlates with markers of immune evasion and with reduced response to immunotherapy. *Science* **2017**, *355*, doi:10.1126/science.aaf8399.